# Lattice-Oriented Catalytic Growth of Graphene Nanoribbons on Heteroepitaxial Nickel Films

**Hiroki Ago,[†,‡,*] Izumi Tanaka,[†] Yui Ogawa,[‡] Rozan Mohamad Yunus,[‡] Masaharu Tsuji,[†,‡] and Hiroki Hibino[§]**

[†]Institute for Materials Chemistry and Engineering (IMCE), Kyushu University, Fukuoka 816-8580, Japan, [‡]Graduate School of Engineering Sciences, Kyushu University, Fukuoka 816-8580, Japan, and [§]NTT Basic Research Laboratories, NTT Corporation, Kanagawa 243-0198, Japan

**ABSTRACT** Graphene nanoribbons (GNRs) are a promising material for electronic applications, because quantum confinement in a one-dimensional nanostructure can potentially open the band gap of graphene. However, it is still a challenge to synthesize high-quality GNRs by a bottom-up approach without relying on lithographic techniques. In this work, we demonstrate lattice-oriented catalytic growth of single-layer GNRs on the surface of a heteroepitaxial Ni film. Catalytic decomposition of a poly(methyl methacrylate) film on the Ni(100) film at 1000 °C gives narrow nanoribbons with widths of 20−30 nm, which are aligned along either [011] or [01$\bar{1}$] directions of the Ni lattice. Furthermore, low-energy electron microscope (LEEM) analysis reveals that orientation of carbon hexagons in these GNRs is highly controlled by the underlying Ni(100) lattice, leading to the formation of zigzag edges. This heteroepitaxial approach would pave a way to synthesize nanoribbons with controlled orientation for future development of electronic devices based on graphene nanostructures.

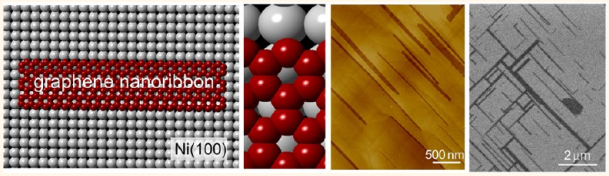


**KEYWORDS:** graphene · nanoribbons · LEEM · epitaxy · zigzag edges

Graphene, a single atomic sheet of carbon hexagons, has attracted great interest due to its high carrier mobility, high thermal conductivity, mechanical flexibility, and optical transparency.[1] These excellent properties promise a wide variety of electronic applications, such as transparent electrodes,[2] touch panels,[3] high frequency transistors,[4] and chemical sensors.[5] For the semiconductor applications of graphene, opening the band gap is a challenging task, as ideal two-dimensional graphene is a zero-gap material.[6] Several methods have been proposed to open the band gap of graphene, such as application of a vertical electric field to double-layer graphene,[7,8] introduction of mechanical strain,[6,9] chemical functionalization,[10] physisorption of organic molecules,[11] and quantum confinement into nanostructures.[12−19] Electron confinement in a one-dimensional nanostructure of graphene, so-called graphene nanoribbons (GNRs), is one promising approach to open the band gap.[12−14] Theoretical investigation suggests that the band gap is inversely proportional to the width of nanoribbons.[14] In addition, the GNRs with zigzag edges are proposed to give a specific edge state which potentially offers exotic electronic properties, such as magnetism originated in localized spins, spin transport, and half metallic property.[12,13,15,16]

The most widely employed method to prepare GNRs is based on a top-down approach, which utilizes lithography and plasma etching or reactive ion etching (RIE) processes.[17−26] Different types of lithographic methods, such as electron beam lithography,[18−23] nanowire templated[24,25] or block-copolymer templated[26] methods, have been demonstrated. Oxygen plasma or RIE treatment is applied to remove uncovered graphene areas, leaving narrow stripes of graphene. Unzipping of carbon nanotubes by either chemical oxidation or plasma oxidation is another approach to prepare GNRs.[27,28] However, these methods inevitably damage edges of the GNRs and sometimes the GNR itself, as observed by enhanced defect-related D-band in the Raman spectrum. In most of the cases, the D-band intensity is higher than that of G-band ($I_D/I_G > 1$) when single-layer graphene is used for the patterning.[19,20] In

* Address correspondence to ago@cm.kyushu-u.ac.jp.

Received for review August 7, 2013 and accepted November 9, 2013.

**Published online November 09, 2013**
**10.1021/nn405122r**

addition, it is difficult to define the edge structure of the nanoribbons prepared by these methods, because the orientation of graphene is unknown and, more importantly, the random edges are produced due to harsh etching processes.[17] Reflecting such disordered edge structures formed by top-down approaches, the carrier transport in these nanoribbons is widely explained by a thermally activated carrier hopping mechanism,[21,23] indicating the top-down synthesized GNR is treated as a series of small graphene fragments mainly due to heavily disordered edge structure.

An alternative method to realize graphene nanoribbon structures is a bottom-up approach. Surface-assisted coupling of molecular precursors into linear polymers gives graphene nanoribbons with armchair edges.[29,30] These GNRs have atomically well-defined structure, as observed by scanning tunneling microscope (STM), but these ribbons are too small to investigate transport properties by making devices on insulating substrates. Chemical vapor deposition (CVD) using meal catalysts is a powerful and effective method to grow single-layer graphene.[31,32] However, two-dimensional (2D) metal catalyst films make it difficult to synthesize one-dimensional (1D) GNRs. Thus, limited works have been demonstrated to grow GNRs by CVD. The CVD growth on the metal catalysts having surface steps or twin boundaries are reported to stimulate the GNR growth.[33,34] Plasma CVD has also been applied to grow GNRs underneath the patterned metal catalyst.[35] However, in these catalytic CVD studies, edge structure of GNRs have not been studied and sometimes the ribbons are very wide (>100 nm).

In this paper, we report a new bottom-up, catalytic growth method of GNRs on a planar heteroepitaxial Ni film. Vacuum annealing of a thin film of poly(methyl methacrylate) on an epitaxial Ni(100) film resulted in the growth of a number of narrow GNRs on the Ni surface, which are aligned along either [011] or [01$\bar{1}$] directions of the Ni. The transferred nanoribbons are found to be high-quality single-layer graphene. In addition, the low-energy electron microscope (LEEM) was performed for as-grown GNR, and we found that all the GNRs have specific hexagon orientations so as to be terminated with zigzag edges regardless of their width. Our bottom-up approach offers a novel facile route to grow single-layer graphene nanoribbons with controlled edge structure for future carbon-based electronics and spintronics.

## RESULTS AND DISCUSSION

For the growth of GNRs, a heteroepitaxial Ni(100) film and PMMA were used as a catalyst and carbon source, respectively. The Ni(100) film was deposited on a MgO(100) single crystalline substrate by sputtering at high temperature (~500 °C). Then, a thin film of PMMA was spin-coated on the Ni(100) surface. Vacuum annealing of the PMMA/Ni/MgO at 1000 °C for 2 min under pressure of $\sim 4 \times 10^{-4}$ Pa followed by rapid cooling resulted in the formation of a number of GNRs on the Ni(100) surface. Figure 1a–c shows SEM images of Ni(100) surface measured after annealing with PMMA. Dark and bright areas correspond to graphene and bare Ni surface with native oxide layer, respectively. A number of narrow dark lines indicate the formation of GNRs. From Figure 1a, one sees that GNRs are aligned only in two directions: parallel to either [011] or [01$\bar{1}$] directions of the Ni film. Although there are variations in width and length, we observed narrow GNRs with 20–50 nm and high aspect ratio >20.

Figure 1d,e shows atomic force microscope (AFM) images of the Ni surface. The AFM images suggest that the graphene is formed inside very shallow trenches. Other images can also be found in the Supporting Information, Figures SI-1 and SI-2. To confirm the growth of graphene inside these narrow and shallow trenches, we transferred graphene onto $SiO_2$/Si substrate by using a standard polymer-mediated transfer technique.[36] We successfully observed the transferred GNRs on the $SiO_2$/Si substrate while maintaining the original orientation, as shown in Figure 1f and Supporting Information, Figure SI-3. We found that the transfer of narrow GNRs is much more difficult than that of uniform single-layer graphene sheets for two reasons; one is the adhesion force of GNRs to $SiO_2$ surface is very weak due to limited contact area. Thus, GNRs, in particular narrow GNRs, were sometimes removed during the dissolution of the polymer support film by acetone. Another reason is the difficulty in removing the polymer film used for the transfer of GNRs when compared with a uniform graphene film. The remaining polymer residue can be seen in Figure 1f. We think that graphene edges tend to bind the polymer support strongly, making it difficult to be removed by acetone. Therefore, special attention, such as slow etching and removal of Cu and the polymer layer, respectively as well as careful handling, was necessary to successfully transfer narrow GNRs from the Ni(100) surface onto the $SiO_2$ surface.

To further confirm the GNRs are formed only inside the trenches appearing on the Ni(100) surface, we measured AFM for an identical location during the transfer. Figure 1h,i shows the AFM images measured before and after the transfer processes, respectively (see also Supporting Information, Figures SI-4 and SI-5). These images verify that the GNRs are formed only inside the narrow and shallow trenches. AFM height profiles are displayed in Figure 1j. Before the transfer there were trenches with the depth of ~1.5 nm. After the transfer, the GNRs with the height of 1–1.5 nm was observed. Although this is relatively higher than the standard AFM height of single-layer graphene sheet

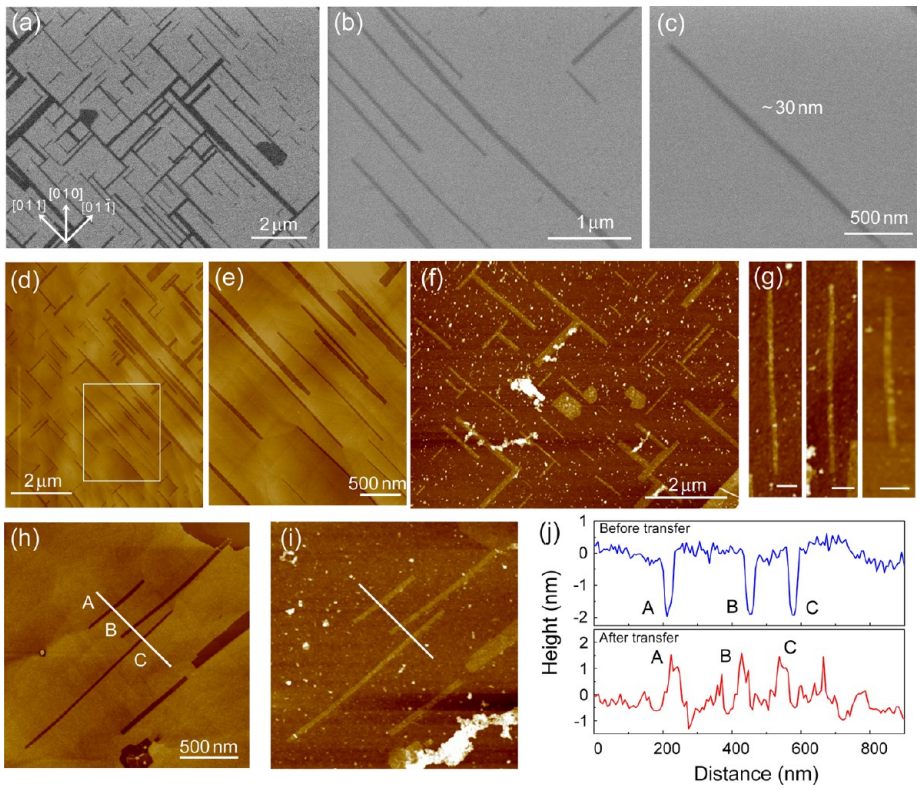


**Figure 1. SEM (a−c) and AFM (d and e) images of as-grown GNRs formed on a heteroepitaxial Ni(100) surface. The dark contrast in (a−c) corresponds to as-grown graphene. (e) Enlarged AFM image shown in a square of (d). (f and g) AFM images of transferred GNRs on $SiO_2$ substrates. All scale bars are 100 nm in (g), and widths of three nanoribbons are around 30 nm. AFM images of the multiple GNRs measured before (h) and after (i) the transfer. (j) Height profile of the AFM along the lines shown in (h) and (i). A, B, and C denote each nanoribbon indicated in (h).**

(~0.8 nm)[37] probably due to PMMA residue, we confirmed that these are single-layer graphene by transmission electron microscopy (TEM), Raman, and LEEM, as shown later. The AFM analysis also indicates that the transferred GNRs seen in Figure 1j have the width of 28−34 nm without tip deconvolution (see Supporting Information, Figure SI-4 for the width measurement). Considering effect of the tip curvature, the actual nanoribbon width can be narrower than these values. We should note that graphene is always observed inside trenches and trenches are always fully covered with graphene. This is confirmed by the SEM/AFM observation for the same areas before and after the graphene transfer (see Figure 1h,i and Supporting Information, Figure SI-5). This result strongly suggests that the graphene develops together with the enlargement of trenches.

Thickness of a Ni(100) film was found to be one of important factors for the formation of nanoscale trenches in which graphene nanoribbons are grown. The Ni film with 100−200 nm was effective to produce the nanoscale trenches. Too thin Ni film with less than 50 nm thickness resulted in the Ni agglomeration, while too thick Ni film, such as 500 nm, did not induce the trench formation.

Moreover, we found that the gradient in the Ni film thickness can increase the yield of nanoribbons. To demonstrate this, we made the patterned Ni catalyst using a metal mask during Ni sputtering at high temperature, as shown in Figure 2a. The height profile measured by a laser microscope (Figure 2b) shows very gradual slope in the Ni film. Figure 2c shows an SEM image taken after the vacuum annealing without a thin PMMA layer, *i.e.*, no carbon source. In that case, neither trenches nor graphene nanoribbons were observed on the Ni surface. This result indicates that the narrow and anisotropic trenches observed on the Ni(100) surface (see Figure 1d,e,h) are induced by the carbon supply from PMMA. As described above, we observed a number of oriented GNRs when we annealed in the presence of PMMA thin film, as shown in Figure 2d,e. In particular, the number of isolated nanoribbons increased toward outside the catalyst pattern with the gradual slope. On the other hand, on the flat areas of the Ni film, large graphene flakes were frequently observed. Therefore, we conclude that gradual change in the Ni film thickness together with external carbon supply result in the formation of graphene nanoribbons inside narrow trenches.

Considering the larger lattice mismatch between Ni and MgO lattices (16%), strain and dislocation are expected to exist in the sputtered Ni(100) film. Such structural disorder induces slippage of the crystal lattices. In most of the fcc metals such as Ni, it is known

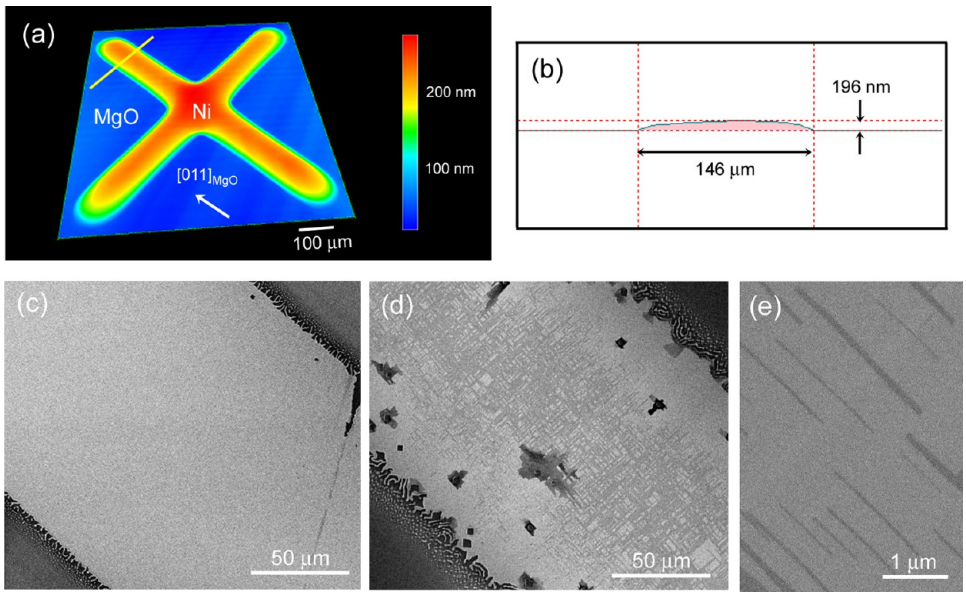


**Figure 2. (a) Height profile of the patterned Ni film deposited on MgO(100) substrate. (b) Cross section of the patterned Ni film. (c) SEM images of the Ni film after annealing without (c) and with (d) PMMA source. (e) Magnified image of (d).**

that slippage occurs along two directions, [011] and [01$\bar{1}$] directions. Thus, this slippage is expected to assist the formation of 1D nanostructures, such as GNRs. We think that local anisotropy in the Ni(100) film, such as a gradient in the Ni film thickness and step/edge structure, also stimulates this anisotropic graphene segregation.

Figure 3a shows a TEM image of cross-section of the as-grown sample. Here, we prepared the specimen normal to the longitudinal axis of nanoribbons with a thickness of around 100 nm by focused-ion beam (FIB). To protect graphene from damage induced by the FIB process, the sample surface was first covered by amorphous carbon, followed by depositing a thick W layer (W layer is not seen in Figure 3a). Electron diffraction from the interface between Ni and MgO indicates that the Ni(100) is epitaxially grown on the MgO(100) substrate (Figure 3b and Supporting Information, Figure SI-6). Reflecting the lattice constants of Ni and MgO crystals ($a_{Ni}$ = 3.52 Å, $a_{MgO}$= 4.21 Å), two types of patterns with the same symmetry were obtained. As shown in Figure 3c,d, a narrow trench with depth of ~0.5 nm was observed on the surface of the Ni film. A graphene layer was observed only inside these shallow trenches with a 32 nm width, as expected from Figure 1. The trench depth varied from 0.5 to 2 nm (Supporting Information, Figure SI-7 shows a deeper trench with ~1 nm), but there is no clear relationship between the trench depth and length/width.

In our catalytic growth of GNRs on the Ni(100), carbon atoms supplied from the PMMA precursor are dissolved in the Ni film, followed by segregation as graphene sheets. The catalytic growth using a polymer film as carbon precursor has already been reported in the previous literature.[38−40] However, these previous works obtained either uniform or nonuniform sheets of single-layer and multilayer graphene without specific nanostructures. The present work shows very unique result that one-dimensional graphene nanostructures can be synthesized on a planar metal film.

Transferred graphene was studied by Raman spectroscopy. Figure 4a is an AFM image of the transferred graphene, where Raman mapping was performed. Here, we used relatively wide nanoribbons (width ~75 nm) to confirm the ribbon structure, because very narrow ribbons are difficult to obtain a clear Raman mapping image due to relatively large laser spot size (~600 nm) compared with the nanoribbon size. The Raman mapping of G-band intensity (Figure 4b) clearly shows linear features, signifying that these aligned stripes are graphene. The G-band intensity is uniform within one ribbon indicating uniformity of our aligned GNRs. When compared with the G- and 2D-bands, the D-band intensity was significantly weaker, indicating the high quality of our graphene nanoribbons. Figure 4c shows the Raman spectra taken for different GNRs. The relative 2D/G band intensity ($I_{2D}/I_G \approx 1.7$) and narrow 2D-bandwidth (30−35 $cm^{-1}$) prove the catalytic growth of single-layer graphene GNRs.[41] We note that the D-band intensity of our transferred GNRs ($I_D/I_G \approx 0.2$) is much weaker than that of the GNRs prepared by top-down methods using oxygen plasma or acid treatments ($I_D/I_G > 1$).[18,19] This means that our GNRs are of high quality because they are gown by a bottom-up method without utilizing any graphene etching processes.

Low energy electron microscope (LEEM) is a powerful tool to analyze graphene grown on metal catalysts, because it gives information on number of layers, orientation of graphene domains, and relative orientation with respect to the underlying metal lattice,

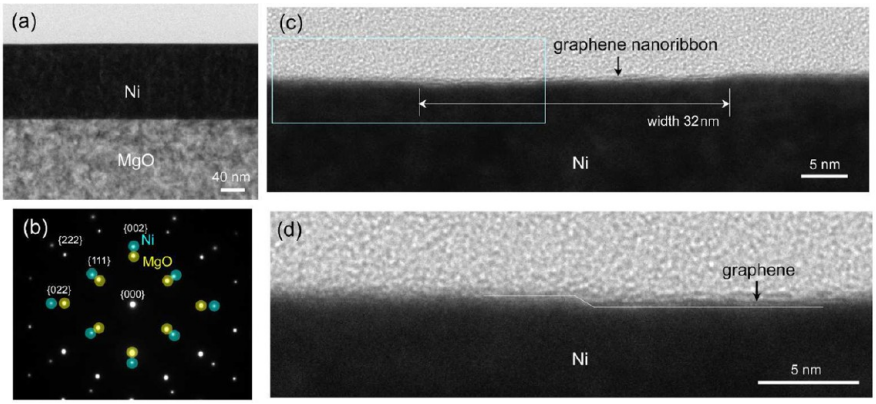


**Figure 3. (a) Cross-sectional TEM image of Ni/MgO(100) substrate after graphene growth. (b) Electron diffraction pattern taken at the interface of Ni and MgO. Blue and yellow circles indicate the diffraction patterns from Ni and MgO, respectively. (c and d) High resolution TEM images of the Ni surface with a graphene nanoribbon. (d) Left edge of the graphene nanoribbon marked as the square in (c).**

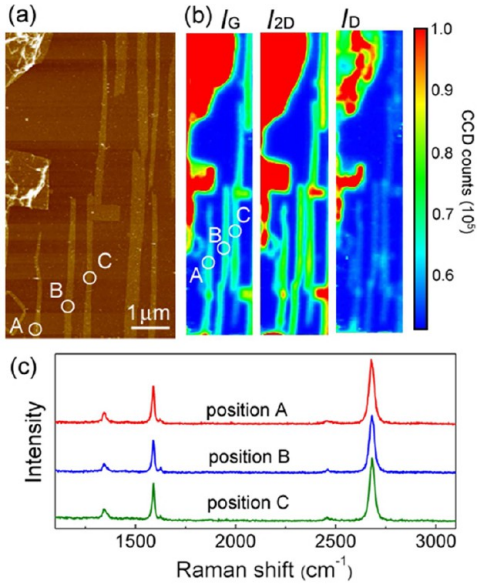


**Figure 4. AFM image (a) and the corresponding Raman mapping images (b) of transferred graphene nanoribbons. The Raman mapping areas is not exactly the same with the AFM scan area. In (b), spatial distributions of G-, D-, and 2D-band intensities are plotted. For clear Raman mapping, relatively wide ribbons were measured; ribbon A has the width ~75 nm. (c) Raman spectra taken at the positions marked in (a) and (b).**

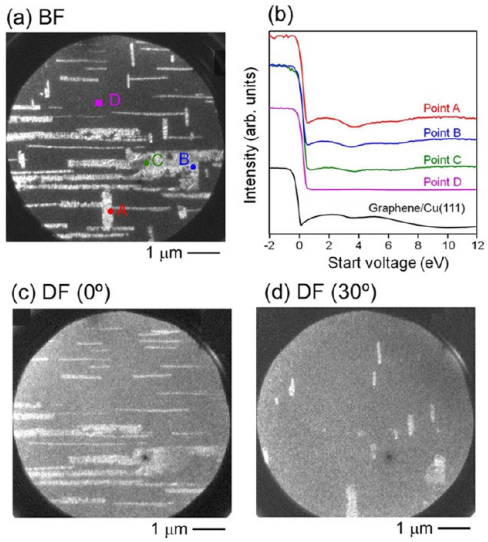


**Figure 5. (a) Bright-field LEEM image of the as-grown GNRs on Ni surface. The electron beam energy was 45 eV. (b) Electron reflectivity spectra measured at different points marked in (a). Position D is bare (but oxidized) Ni surface, thus showing no specific signal originating in graphene. The profile of single-layer graphene film grown on Cu(111)[43] is also shown for comparison. Corresponding dark-filed LEEM images taken with the azimuths of the incident electron beam of 0° (c) and 30° (d). The electron beam energies were 58 eV.**

without transferring onto insulating substrates.[42,43] Figure 5a shows a bright-field (BF) image of the as-grown graphene on Ni(100) surface. Due to spatial resolution limit of the LEEM (~20 nm), it was difficult to accurately determine the nanoribbon width, but we could clearly observe the graphene nanoribbons with around 30−40 nm width in the BF-LEEM image (detailed analysis of the nanoribbon width by LEEM images is shown in Supporting Information, Figure SI-8). Electron reflectivity spectra measured at the four different areas of Figure 5a are displayed in Figure 5b. For comparison, the data of the uniform single-layer graphene grown on Cu(111) is also indicated by a black line.[43] The single-layer graphene on Cu(111) shows a specific profile with two broad reflection peaks at ~2 and ~5 eV, although this intensity change is smaller than the characteristic intensity changes used to determine the number of layers for the double-layer and triple-layer graphene on Cu(111).[44] Such a slightly undulating profile was also observed at points A, B, and C, providing the growth of single-layer graphene nanoribbons. On the other hand, the dark region, D, showed no reflection peak due to bare (but oxidized) Ni surface without a graphene over layer.

Next, the same sample was subjected to the dark-field (DF) measurement to study the orientation of

carbon hexagons comprising the graphene lattice. Figure 5c,d shows the DF-LEEM images taken with two diffraction conditions, 0° and 30°. The DF-LEEM images were obtained by inclining the incident electron beam from the surface normal so as to let the first-order diffraction beams of graphene come out normally to the surface. In Figure 5c, only the horizontally aligned nanoribbons appeared bright. This DF image indicates these horizontally aligned GNRs have the same hexagon orientation regardless of the ribbon width. When we switched the diffraction condition, 30°-rotations against Figure 5c, the GNRs aligned only in vertical direction became bright (Figure 5d). This indicates that the carbon hexagon orientation of these vertically aligned GNRs is rotated by 30° (or 90°) with respect to the horizontally aligned GNRs. In this observed area, the density of the horizontally oriented GNRs is higher than that of the vertically oriented ones, and the aspect ratio of the former ribbons is higher than the latter ones, but such structural difference is dependent on the measured position.

To get more information on the orientation of specific nanoribbons, selected-area electron diffraction was performed, as shown in Figure 6 and Supporting Information, Figure SI-10. Figure 6a and 6c show the BF-LEEM image of a very wide ribbon and the corresponding diffraction pattern, respectively. From the relative orientation of the graphene and the diffraction pattern, we conclude that graphene hexagons are oriented so as to have its zigzag direction parallel to the long axis of the graphene ribbon. This strongly suggests the growth of GNRs terminated with zigzag edges. Much narrower nanoribbons were also measured, as presented in Figure 6b,d. In this area, there are mainly two orthogonal GNRs. Reflecting the presence of two orthogonal GNRs in the area, we observed two sets of weak hexagonal diffraction patterns (Figure 6d), which can be assigned to Gr-A and Gr-B marked in Figure 6b. In Figure 6d, the diffraction from the bare Ni surface was also obtained because the GNRs occupy a small portion of the measured area. Although the Ni surface can be easily oxidized after exposing air when transferred to the LEEM chamber, the Ni(100) lattice partially remained within the depth of detectable by the LEEM (typically ~1 nm).

On the basis of the LEEM results, the relative orientation of graphene lattice with respect to the Ni(100) lattice is determined, as illustrated in Figure 7b. The GNRs are aligned along either [011] or [01$\bar{1}$] direction of the Ni surface with zigzag edges. We can see that one of the C−C bonds of each GNR is parallel to one of the Ni−Ni bonds. This relative configuration is consistent with our previous observation of a sheet of single-layer graphene grown on an epitaxial Cu(100) film at 1000 °C.[42] It is interesting to note that zigzag edges are widely observed in CVD-grown hexagonal graphene domains.[45,46] The previous experimental observations

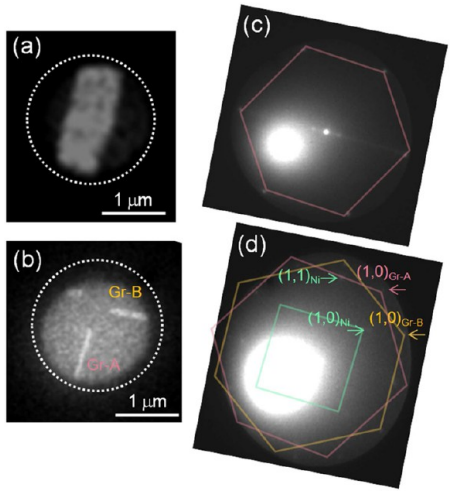


**Figure 6. Bright-field LEEM image (a) and the corresponding diffraction pattern (c) taken for a wide ribbon. (b and d) Bright-field LEEM and diffraction pattern of two orthogonal narrow nanoribbons. The diffraction patterns were obtained at electron energy of 40 eV. Only one set of hexagonal diffraction pattern was observed for one wide ribbon (c), while two orthogonal nanoribbons gave two sets of hexagonal diffraction patterns rotated by 30° (d). Green square shows the diffraction from the exposed Ni(100) surface, which allows us to determine the relative orientation of the graphene nanoribbons with respect to the Ni(100) lattice. Diffraction patterns without the guide lines are shown in Supporting Information, Figure SI-9.**

of zigzag edges in these hexagonal domains infer that the growth rate of armchair edges is faster than zigzag edges so that a hexagonal domain shape appears. We think that this growth rate difference can also be applied to our graphene nanoribbons. Because of the square lattice of the Ni(100) plane, initial graphene nuclei may have square shape confined in the square trenches (Figure 7a). During the graphene growth, these graphene nuclei can potentially extend in two directions, [011] or [01$\bar{1}$], which are crystallographically equivalent. However, as the graphene grows while exposing zigzag edges whose growth rate is slower than armchair edges, one-dimensional nanoribbon structure appears on the Ni(100) surface by suppressing the simple enlargement of square pits. Graphene edges are also known to be influenced by hydrogen gas supplied during CVD growth, modifying the domain structure of single-layer graphene mainly due to hydrogen-assisted graphene ethcing.[47] However, in our case, we only annealed the PMMA film on Ni(100) in high vacuum without any gas flow so it is unlikely that the hydrogen-etching plays a major role in our nanoribbon growth.

From the Raman study of exfoliated graphene flakes, it is reported that pure zigzag edges do not show D-band.[48] However, our graphene nanoribbons showed a weak but clear D-band with a relative ratio of $I_D/I_G \approx 0.2$ (see Figure 4c). We think that the graphene nanoribbons are more reactive than basal plane so that the edges can be oxidized (or damaged) during the graphene transfer

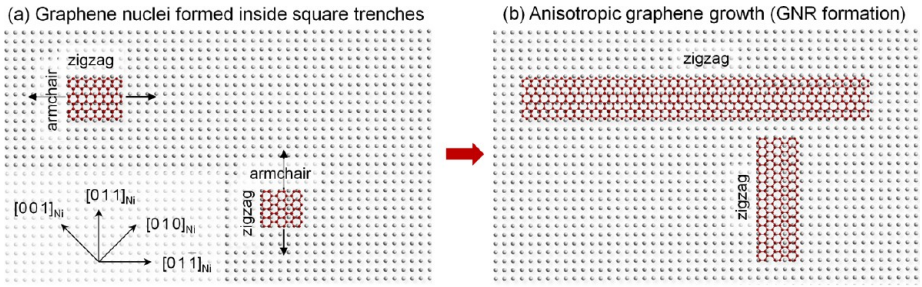


**Figure 7. Growth mechanism of GNRs on Ni(100) surface. The orientations of carbon hexagons of graphene with respect to the Ni(100) lattice are determined from the LEEM measurements. (a) In the initial stage, square graphene domains are formed due to the square Ni(100) lattice. (b) During the graphene growth, graphene extends in specific directions, forming nanoribbon structure. As illustrated in (b), two nanoribbons can have zigzag edges even though they are rotated each other by 90°, as confirmed by LEEM (see Figures 5 and 6, and Supporting Information, Figure SI-10).**

process which involves Ni etching. Also, even though the GNRs are oriented on the Ni(100) lattice so as to have zigzag edges, the actual edges may partially contain armchair edges. It should be noted that clear D-band has also been observed for edges of large hexagonal graphene domains with zigzag edges grown by CVD.[45,46,49]

We previously reported the selective graphene growth inside large $\mu$m-sized square-shaped pits formed on heteroepitaxial $\beta$-Co(100) and Ni(100) films when annealed with a polymer film.[38] The formation of these square pits was explained by the lattice mismatch between the metal film and MgO(100) substrate. As discussed above, the structural anisotropy in the Ni(100) film can also contribute the one-dimensional nanostructure formation. We note that these zigzag edges may give unique phenomena originating in the localized states, and further study is necessary to understand the edge state of our oriented zigzag nanoribbons and the interface between the sidewall of Ni trenches and graphene edges.

Our growth method does not require any post-growth lithographic processes, and the nanoribbons show high crystallinity with low defects. Also, this is a unique synthesis method, because it utilizes the square lattice of the Ni(100) surface. The lattice-oriented growth enables the edge selective growth of zigzag GNRs which should be interesting for spintronics and other exotic physical properties as well as semiconductor applications.[12,13,15,16] Although further reduction of the nanoribbon width and improvement of the uniformity are required, our novel approach of growing one-dimensional ribbon structure is promising and useful for highly controlled growth of graphene nanostructures.

## CONCLUSIONS

Single-layer GNRs are grown on a heteroepitaxial Ni(100) film by catalytic decomposition of a PMMA film. The orientation of these nanoribbons are strongly related with the Ni(100) lattice, indicating epitaxial growth of GNRs. LEEM measurements reveal that these aligned GNRs have specific hexagon orientations with respect to longitudinal axis, signifying the growth of zigzag edges GNRs regardless of ribbon width. Lattice mismatch of the Ni(100) film and MgO(100) substrate and the edge-dependent graphene growth rate are suggested to give such unique nanostructure made of graphene. Our epitaxial growth of graphene nanoribbons is believed to offer a new direction of synthesizing high-quality, graphene nanostructures with controlled edges and provides a new platform with unique physical and chemical properties.

## EXPERIMENTAL SECTION

**GNR Synthesis.** We used MgO(100) single crystalline substrates to deposit epitaxial Ni(100) films. Ni films with 80−200 nm thickness were deposited by radio frequency (RF) magnetron sputtering while heating MgO substrates at 500 °C. This high sputtering temperature was essential to produce a highly crystalline Ni(100) film, as demonstrated previously for epitaxial Co films.[36] Patterning of the Ni film by sputtering through a metal mask, which creates a gradual change in the Ni thickness, was also effective to increase a GNR yield (see Figure 2a,b for the actual Ni pattern). Dilute toluene solution of poly(methyl methacrylate) (PMMA purchased from Aldrich, 0.025 wt %) was spin-coated onto the Ni film. To grow graphene on Ni surface, the PMMA coated Ni(100) substrate was annealed in vacuum ($\sim 4 \times 10^{-4}$ Pa) at 1000 °C for 2 min using an infrared furnace (ULVAC, MILA-3000). The typical heating and cooling rates were 200 °C/min and 200 °C/s, respectively.

**Transfer of Graphene.** For the transfer of graphene nanoribbons grown on Ni(100) film, the Ni surface was covered with a protecting PMMA film by spin coating, followed by attaching thermal tape (Revalpha, Nitto-Denko). After removing the Ni film by immersing in $FeCl_3$ aqueous solution (1 M), the graphene stack was transferred onto a $SiO_2$/Si substrate. Finally, the thermal tape and PMMA film were removed by heat treatment and dipping into hot acetone solution, respectively.

**Characterization.** Atomic force microscope (AFM, Bruker Nanoscope V) and scanning electron microscope (SEM, HITACHI S-4800) were used to image the Ni surface and the transferred graphene nanoribbons. The height profile of the Ni pattern shown in Figure 2 was measured by a 3 CCD confocal microscope (Lasertech Co., OPTELICS HI200). Confocal Raman spectroscopy (Tokyo Instruments, Nanofinder30) was applied to the nanoribbons transferred on a $SiO_2$/Si substrate with a 532 nm excitation. TEM images were measured with a HITACHI H-9500 for the sample sliced with a focused-ion-beam (FIB, HITACHI

NB5000). Crystal orientations of as-grown graphene were characterized by Elmitec LEEM III under ultrahigh vacuum. To remove impurity on the surface, we annealed a sample in vacuum before the LEEM measurement.

*Conflict of Interest:* The authors declare no competing financial interest.

*Supporting Information Available:* As-grown graphene on heteroepitaxial Ni(100) surface; SEM and AFM images of the as-grown graphene on Ni(100); AFM images of transferred GNRs on $SiO_2$ surface and detailed height profiles; complementary information of Figure 2; cross-sectional TEM images of GNRs with 64 nm width; analysis of nanoribbon width by LEEM; selected-area LEEM diffraction analysis; BF-LEEM images of the high-density GNRs. This material is available free of charge *via* the Internet at http://pubs.acs.org.

*Acknowledgment.* This work was supported by JSPS Funding Program for Next Generation World-Leading Researchers (NEXT Program, #GR075). Y. Ogawa acknowledges the support from Grant-in-Aid for a JSPS Fellow.

## REFERENCES AND NOTES

1. Geim, A. K.; Novoselov, K. S. The Rise of Graphene. *Nat. Mater.* **2007**, *6*, 183–191.
2. Han, T. H.; Lee, Y.; Choi, M. R.; Woo, S. H.; Bae, S. H.; Hong, B. H.; Ahn, J. H.; Lee, T. W. Extremely Efficient Flexible Organic Light-Emitting Diodes with Modified Graphene Anode. *Nat. Photonics* **2012**, *6*, 105–110.
3. Bae, S.; Kim, H.; Lee, Y.; Xu, X.; Park, J. S.; Zheng, Y.; Balakrishnan, J.; Lei, T.; Kim, H. R.; Song, Y. I.; *et al.* Roll-to-Roll Production of 30-in. Graphene Films for Transparent Electrodes. *Nat. Nanotechnol.* **2010**, *5*, 574–578.
4. Lin, Y. M.; Dimitrakopoulos, C.; Jenkins, K. A.; Farmer, D. B.; Chiu, H. Y.; Grill, A.; Avouris, P. 100-GHz Transistors from Wafer-Scale Epitaxial Graphene. *Science* **2010**, *327*, 662.
5. Ohno, Y.; Maehashi, K.; Yamashiro, Y.; Matsumoto, K. Electrolyte-Gated Graphene Field-Effect Transistors for Detecting pH and Protein Adsorption. *Nano Lett.* **2009**, *9*, 3318–3322.
6. Zhan, D.; Yan, J.; Lai, L.; Ni, Z.; Liu, L.; Shen, Z. Engineering the Electronic Structure of Graphene. *Adv. Mater.* **2012**, *24*, 4055–4069.
7. Oostinga, J. B.; Heersche, H. B.; Liu, X.; Morpurgo, A. F.; Vandersypen, L. M. K. Gate-Induced Insulating State in Bilayer Graphene Devices. *Nat. Mater.* **2008**, *7*, 151–157.
8. Zhang, Y.; Tang, T. T.; Girit, C.; Hao, Z.; Martin, M. C.; Zettl, A.; Crommie, M. F.; Shen, Y. R.; Wang, F. Direct Observation of a Widely Tunable Bandgap in Bilayer Graphene. *Nature* **2009**, *459*, 820–823.
9. Guinea, F.; Katsnelson, M. I.; Geim, A. K. Energy Gaps and a Zero-Field Quantum Hall Effect in Graphene by Strain Engineering. *Nat. Phys.* **2010**, *6*, 30–33.
10. Loh, K. P.; Bao, Q.; Ang, P. K.; Yang, J. The Chemistry of Graphene. *J. Mater. Chem.* **2010**, *20*, 2277–2289.
11. Kozlov, S. M.; Viñes, F.; Görling, A. Bandgap Engineering of Graphene by Physisorbed Adsorbates. *Adv. Mater.* **2011**, *23*, 2638–2643.
12. Tanaka, K.; Yamashita, S.; Yamabe, H.; Yamabe, T. Electronic Properties of One-Dimensional Graphite Family. *Synth. Met.* **1987**, *17*, 143–148.
13. Nakada, K.; Fujita, M.; Dresselhaus, G.; Dresselhaus, M. S. Edge State in Graphene Ribbons: Nanometer Size Effect and Edge Shape Dependence. *Phys. Rev. B* **1996**, *54*, 17954–17961.
14. Yang, L.; Park, C. H.; Son, Y. W.; Cohen, M. L.; Louie, S. G. Quasiparticle Energies and Band Gaps in Graphene Nanoribbons. *Phys. Rev. Lett.* **2007**, *99*, No. 186801.
15. Son, Y. W.; Cohen, M. L.; Louie, S. G. Half-Metallic Graphene Nanoribbons. *Nature* **2006**, *444*, 347–349.
16. Dutta, S.; Wakabayashi, K. Tuning Charge and Spin Excitations in Zigzag Edge Nanographene Ribbons. *Sci. Rep.* **2012**, *2*, No. 519.
17. Ma, L.; Wang, J.; Ding, F. Recent Progress and Challenges in Graphene Nanoribbon Synthesis. *Chem. Phys. Chem.* **2013**, *14*, 47–54.
18. Han, M. Y.; Brant, J. C.; Kim, P. Electron Transport in Disordered Graphene Nanoribbons. *Phys. Rev. Lett.* **2010**, *104*, No. 56801.
19. Wang, X.; Dai, H. Etching and Narrowing of Graphene from the Edges. *Nat. Chem.* **2010**, *2*, 661–665.
20. Ryu, S.; Maultzsch, J.; Han, M. Y.; Kim, P.; Brus, L. E. Raman Spectroscopy of Lithographically Patterned Graphene Nanoribbons. *ACS Nano* **2011**, *5*, 4123–4130.
21. Nakaharai, S.; Iijima, T.; Ogawa, S.; Miyazaki, H.; Li, S.; Tsukagoshi, K.; Sato, S.; Yokoyama, N. Gate-Controlled P−I−N Junction Switching Device with Graphene Nanoribbon. *Appl. Phys. Exp.* **2012**, *5*, No. 15101.
22. Bischoff, D.; Krähenmann, T.; Dröscher, S.; Gruner, M. A.; Barraud, C.; Ihn, T.; Ensslin, K. Reactive-Ion-Etched Graphene Nanoribbons on a Hexagonal Boron Nitride Substrate. *Appl. Phys. Lett.* **2012**, *101*, No. 203103.
23. Hwang, W. S.; Tahy, K.; Li, X.; Xing, H.; Seabaugh, A. C.; Sung, C. Y.; Jena, D. Transport Properties of Graphene Nanoribbon Transistors on Chemical-Vapor-Deposition Grown Wafer-Scale Graphene. *Appl. Phys. Lett.* **2012**, *100*, No. 203107.
24. Bai, J.; Duan, X.; Huang, Y. Rational Fabrication of Graphene Nanoribbons Using a Nanowire Etch Mask. *Nano Lett.* **2009**, *9*, 2083–2087.
25. Stützel, E. U.; Dufaux, T.; Sagar, A.; Rauschenbach, S.; Balasubramanian, K.; Burghard, M.; Kern, K. Spatially Resolved Photocurrents in Graphene Nanoribbon Devices. *Appl. Phys. Lett.* **2013**, *102*, No. 43106.
26. Liang, X.; Wi, S. Transport Characteristics of Multichannel Transistors Made from Densely Aligned Sub-10 nm Half-Pitch Graphene Nanoribbons. *ACS Nano* **2012**, *6*, 9700–9710.
27. Kosynkin, D. V.; Higginbotham, A. L.; Sinitskii, A.; Lomeda, J. R.; Dimiev, A.; Price, B. K.; Tour, J. M. Longitudinal Unzipping of Carbon Nanotubes To Form Graphene Nanoribbons. *Nature* **2009**, *458*, 872–876.
28. Jiao, L.; Zhang, L.; Wang, X.; Diankov, G.; Dai, H. Narrow Graphene Nanoribbons from Carbon Nanotubes. *Nature* **2009**, *458*, 877–880.
29. Cai, J.; Ruffieux, P.; Jaafar, R.; Bieri, M.; Braun, T.; Blankenburg, S.; Muoth, M.; Seitsonen, A. P.; Saleh, M.; Feng, X.; *et al.* Atomically Precise Bottom-Up Fabrication of Graphene Nanoribbons. *Nature* **2010**, *466*, 470–473.
30. Huang, H.; Wei, D.; Sun, J.; Wong, S. L.; Feng, Y. P.; Neto, A. H. C.; Wee, A. T. S. Spatially Resolved Electronic Structures of Atomically Precise Armchair Graphene Nanoribbons. *Sci. Rep.* **2012**, *2*, No. 983.
31. Mattevi, C.; Kim, H.; Chhowalla, M. A Review of Chemical Vapour Deposition of Graphene on Copper. *J. Mater. Chem.* **2011**, *21*, 3324–3334.
32. Ago, H.; Ogawa, Y.; Tsuji, M.; Mizuno, S.; Hibino, H. Catalytic Growth of Graphene: Toward Large-Area Single-Crystalline Graphene. *J. Phys. Chem. Lett.* **2012**, *3*, 2228–2236.
33. Ago, H.; Ito, Y.; Tsuji, M.; Ikeda, K. Step-Templated CVD Growth of Aligned Graphene Nanoribbons Supported by Single-Layer Graphene Film. *Nanoscale* **2012**, *4*, 5178–5182.
34. Hayashi, K.; Sato, S.; Ikeda, M.; Kaneta, C.; Yokoyama, N. Selective Graphene Formation on Copper Twin Crystals. *J. Am. Chem. Soc.* **2012**, *134*, 12492–12498.
35. Kato, T.; Hatakeyama, R. Site- and Alignment-Controlled Growth of Graphene Nanoribbons from Nickel Nanobars. *Nat. Nanotechnol.* **2012**, *7*, 651–656.
36. Ago, H.; Ito, Y.; Mizuta, N.; Yoshida, K.; Hu, B.; Orofeo, C. M.; Tsuji, M.; Ikeda, K.; Mizuno, S. Epitaxial Chemical Vapor Deposition Growth of Single-Layer Graphene over Cobalt Film Crystallized on Sapphire. *ACS Nano* **2010**, *4*, 7407–7414.
37. Koh, Y. K.; Bae, M. H.; Cahill, D. G.; Pop, E. Reliably Counting Atomic Planes of Few-Layer Graphene ($n > 4$). *ACS Nano* **2011**, *5*, 269–274.
38. Ago, H.; Tanaka, I.; Orofeo, C. M.; Tsuji, M.; Ikeda, K. Patterned Growth of Graphene over Epitaxial Catalyst. *Small* **2010**, *6*, 1226–1233.

39. Suzuki, S.; Takei, Y.; Furukawa, K.; Hibino, H. Graphene Growth from a Spin-Coated Polymer without a Reactive Gas. *Appl. Phys. Exp.* **2011**, *4*, No. 65102.
40. Sun, Z.; Yan, Z.; Yao, J.; Beitler, E.; Zhu, Y.; Tour, J. M. Growth of Graphene from Solid Carbon Sources. *Nature* **2010**, *468*, 549–552.
41. Ferrari, A. C.; Meyer, J. C.; Scardaci, V.; Casiraghi, C.; Lazzeri, M.; Mauri, F.; Piscanec, S.; Jiang, D.; Novoselov, K. S.; Roth, S.; *et al.* Raman Spectrum of Graphene and Graphene Layers. *Phys. Rev. Lett.* **2006**, *97*, No. 187401.
42. Hibino, H.; Kageshima, H.; Maeda, F.; Nagase, M.; Kobayashi, Y.; Yamaguchi, H. Microscopic Thickness Determination of Thin Graphite Films Formed on SiC from Quantized Oscillation in Reflectivity of Low-Energy Electrons. *Phys. Rev. B* **2008**, *77*, No. 75413.
43. Ogawa, Y.; Hu, B.; Orofeo, C. M.; Tsuji, M.; Ikeda, K.; Mizuno, S.; Hibino, H.; Ago, H. Domain Structure and Boundary in Single-Layer Graphene Grown on Cu(111) and Cu(100) Films. *J. Phys. Chem. Lett.* **2012**, *3*, 219–226.
44. Srivastava, N.; Gao, Q.; Widom, M.; Feenstra, R. M.; Nie, S.; McCarty, K. F.; Vlassiouk, I. V. Low-Energy Electron Reflectivity of Graphene on Copper and Other Substrates. *Phys. Rev. B* **2013**, *87*, No. 245414.
45. Yu, Q.; Jauregui, L. A.; Wu, W.; Colby, R.; Tian, J.; Su, Z.; Cao, H.; Liu, Z.; Pandey, D.; Wei, D.; *et al.* Control and Characterization of Individual Grains and Grain Boundaries in Graphene Grown by Chemical Vapour Deposition. *Nat. Mater.* **2011**, *10*, 443–449.
46. Ago, H.; Kawahara, K.; Ogawa, Y.; Tanoue, S.; Bissett, M. A.; Tsuji, M.; Sakaguchi, H.; Koch, R. J.; Fromm, F.; Seyller, T.; *et al.* Epitaxial Growth and Electronic Properties of Large Hexagonal Graphene Domains on Cu(111) Thin Film. *Appl. Phys. Exp.* **2013**, *6*, No. 75101.
47. Vlassiouk, I.; Regmi, M.; Fulvio, P.; Dai, S.; Datskos, P.; Eres, G.; Smirnov, S. Role of Hydrogen in Chemical Vapor Deposition Growth of Large Single-Crystal Graphene. *ACS Nano* **2011**, *5*, 6069–6076.
48. Krauss, B.; Nemes-Incze, P.; Skakalova, V.; Biro, L. P.; von Klitzing, K.; Smet, J. H. Raman Scattering at Pure Graphene Zigzag Edges. *Nano Lett.* **2010**, *10*, 4544–4548.
49. Yan, Z.; Lin, J.; Peng, Z.; Sun, Z.; Zhu, Y.; Li, L.; Xiang, C.; Samuel, E. L.; Kittrell, C.; Tour, J. M. Toward the Synthesis of Wafer-Scale Single-Crystal Graphene on Copper Foils. *ACS Nano* **2012**, *6*, 9110–9117.